

RSC Advances



This is an *Accepted Manuscript*, which has been through the Royal Society of Chemistry peer review process and has been accepted for publication.

Accepted Manuscripts are published online shortly after acceptance, before technical editing, formatting and proof reading. Using this free service, authors can make their results available to the community, in citable form, before we publish the edited article. This *Accepted Manuscript* will be replaced by the edited, formatted and paginated article as soon as this is available.

You can find more information about *Accepted Manuscripts* in the [Information for Authors](#).

Please note that technical editing may introduce minor changes to the text and/or graphics, which may alter content. The journal's standard [Terms & Conditions](#) and the [Ethical guidelines](#) still apply. In no event shall the Royal Society of Chemistry be held responsible for any errors or omissions in this *Accepted Manuscript* or any consequences arising from the use of any information it contains.

Ammonia selective catalytic reduction of NO over Ce-Fe /Cu-SSZ-13 catalysts

Xiaojiao Liu ^{a,b,c}, Yonghong Li ^{a,b,c*}, Ranran Zhang ^{a,b,c}

a. Key Lab for Green Chemical Technology of Ministry of Education, School of Chemical Engineering and Technology, Tianjin University, Weijin Road 92, Tianjin 300072, China

b. National Engineering Research Center for Distillation Technology, Tianjin 300072, China

c. Collaborative Innovation Center of Chemical Science and Engineering (Tianjin), Tianjin 300072, China

*Corresponding author, Tel.: +86 022 27404701-8858; Fax: +86 022 27404705

E-mail: yhli@tju.edu.cn.

Postal address: School of Chemical Engineering and Technology, Tianjin University, Weijin Road 92, Tianjin 300072, China

Abstract

A series of CHA-type trimetallic composite zeolites of Ce_x-Fe_y/Cu-SSZ-13 catalysts were prepared by the one-pot synthesized Cu-SSZ-13 and subsequent ion-exchange with Fe³⁺ and Ce³⁺. The catalysts were characterized including TEM, XRD, XPS, SEM and BET. Their catalytic performances for selective catalytic reduction of NO with NH₃ were investigated. The results of XRD revealed that the crystal structure of zeolite Ce-Fe /Cu-SSZ-13 is the same as Cu-SSZ-13. It was known that larger specific surface areas and smaller pore size were in favor of catalytic reaction from the results of BET and catalytic performance tests. Among the prepared Ce_x-Fe_y/Cu-SSZ-13 catalysts, Ce_{0.017}-Fe_{0.017}/Cu-SSZ-13 displayed the best SCR performance. The NO conversion was more than 90% between 200 and 500 °C. N₂ selectivity was above 98% within the wider temperature

range of 150-550 °C. In addition, the catalyst demonstrated sulfur-water tolerance and effective resistance against high space velocity. The phenomena suggest that synergistic effects of Cu, Fe and Ce species improve the SCR performances and make Ce-Fe/Cu-SSZ-13 catalyst as a promising candidate for NH₃-SCR technology.

Key words: selective catalytic reduction; NO_x-removal; SSZ-13; zeolite modification

Introduction

Nitrogen oxides emitted by diesel engines are a major kind of air pollutants that are responsible for acid rain, photochemical smog and ozone depletion. With legislation of NO_x emissions becoming more and more stringent, it is urgent to find an effective way to remove such pollutants from the exhaust. Nowadays, one of the most promising technologies to eliminate the NO_x pollution is selective catalytic reduction (SCR) of NO_x with ammonia.¹ Recently, Cu/zeolite catalysts with chabazite (CHA) crystal structure, such as Cu-SSZ-13, has received much attention^{2,3}. Cu-SSZ-13 prepared by an ion-exchange method is much more active, selective and hydrothermally stable than Cu-beta and Cu-ZSM-5.^{4,5} However, the template N,N,N-trimethyl-1-adamantammonium hydroxide (TMAdaOH) used in the synthesis of SSZ-13 by Zones^{6,7} is rather expensive. Therefore, it is desirable to find a substitute for the template TMAdaOH. Nuria et al⁸ suggested that the low-cost methodologies to synthesize Cu-containing CHA catalysts using tetraethylammonium (TEA) as organic structure directing agent (OSDA) could be competitive and attractive for NH₃-SCR of NO_x. In addition, an economical way for SSZ-13 preparation with the essentially cheap choline chloride as template has been attempted by Chen et al⁹ and the as-synthesized SSZ-13 zeolite, ion-exchanged by copper nitrate solution, exhibited excellent SCR performance. Furthermore, Ren et al¹⁰ first used low-cost copper-amine complex as

the template for one-pot synthesis of Cu-SSZ-13 zeolite. Later, Xie et al¹¹ had further improved the synthesis method of Cu-SSZ-13 catalyst and indicated that the one-pot synthesized Cu-SSZ-13 catalyst was a promising candidate for the NO_x elimination from diesel engine exhaust.

At present, more and more researchers are interested in heterobimetallic zeolites because of the complementary advantages and synergistic effects. In order to further improve the activity of the one-pot synthesized Cu-SSZ-13 catalyst, Zhang et al¹² prepared Fe_x/Cu-SSZ-13 catalysts by incorporating Fe³⁺ into Cu-SSZ-13 and the catalysts exhibited high NH₃-SCR activity, excellent N₂ selectivity, robust hydrothermal stability and good tolerance to high space velocity. Ceria has been widely used as an additive of various catalysts because of its excellent oxygen storage capacity and high redox ability via Ce⁴⁺ to Ce³⁺ transition¹³⁻¹⁵. Herein, we attempt to modify the Cu/SSZ-13 catalyst with both iron and cerium to develop a more efficient NH₃-SCR catalyst for the potential application in diesel engine exhaust treatment. In this study, the effects of Fe/Ce ratio, gas hourly space velocity (GHSV) and the concentration of O₂ on the activities for NO reduction are systematically investigated. In addition, the tolerance of the catalyst to H₂O, SO₂ and CO₂ was studied as well. The catalysts were further characterized through X-ray powder diffraction (XRD), transmission electron microscope (TEM), N₂ adsorption-desorption (BET), scanning electron microscope (SEM) and X-ray photoelectron spectra (XPS).

Experimental

Preparation of Ce-Fe /Cu-SSZ-13 catalysts

Cu-SSZ-13 was synthesized by one-pot hydrothermal synthesis method as reported by Zhang¹². Ce_x-Fe_y /Cu-SSZ-13 catalysts were prepared by subsequent aqueous ion-exchange method. The specific steps are as follows: A certain amount of Cu-SSZ-13 was slowly added into

Fe(NO₃)₃•9H₂O solution, with constant stirring at 80 °C for 8hrs. The formed precipitate was washed by deionized water followed by drying at 110 °C and then exchanged with Ce(NO₃)₃•6H₂O solution. Finally, the sample was calcined at 550 °C for 5hrs. We chose the optimum concentration of Fe(NO₃)₃•9H₂O solution at 0.017 mol/L according to the literature reported by Zhang¹² and obtained a series of Ce_x-Fe_y /Cu-SSZ-13 catalysts through changing the concentration of Ce(NO₃)₃•6H₂O. The x and y represent concentration (unit: mol/L) of the Ce(NO₃)₃•6H₂O solution and Fe(NO₃)₃•9H₂O solution respectively. The metal weight percentages in the catalysts were measured by ICP analysis. All chemicals used were purchased from Tianjin Huadong Reagent Factory.

Activity measurements

The “standard NH₃-SCR” experiments were performed in a fixed bed reactor (inner diameter 5mm). The simulated exhaust gases were composed of 500 ppm NO, 500 ppm NH₃, 5 vol% O₂, 5 vol% H₂O (when used), 100 ppm SO₂ (when used), 5 vol% CO₂ (when used) and balance N₂. The total flow rate was 300 mL/min and thus a GHSV from 60000 h⁻¹ to 300000 h⁻¹ was obtained by changing the volume of the catalyst. The water vapor was injected by a pump (LSP01-1A, Longer Pump Inc.) and an evaporator. A K-type thermocouple was inserted into the center of catalyst bed from the bottom of the reactor and it was connected to a temperature programmed control instrument to monitor the reaction temperature. The concentration of NH₃, NO, NO₂ and N₂O were measured by a Thermo Nicolet IS10 Fourier-transform infrared (FTIR) spectrometer. NO conversion and N₂ selectivity of NH₃-SCR reaction were defined as:

$$\text{NO conversion} = (1 - [\text{NO}]_{\text{outlet}} / [\text{NO}]_{\text{inlet}}) \times 100\%;$$

$$\text{N}_2 \text{ selectivity} = (([\text{NH}_3]_{\text{inlet}} - [\text{NO}]_{\text{outlet}} - [\text{NO}_2]_{\text{outlet}} - 2[\text{N}_2\text{O}]_{\text{outlet}} - [\text{NH}_3]_{\text{outlet}}) / ([\text{NH}_3]_{\text{inlet}} - [\text{NH}_3]_{\text{outlet}}))$$

×100%

Characterizations

Powder XRD patterns were obtained by a D8-Focus X-ray diffractometer with Cu K α radiation (40 kV, 40 mA, $\lambda=0.15418$ nm). Diffractometer data were obtained with a step size of 5° for 2 θ values from 5° to 40°.

Nitrogen adsorption/desorption isotherms was measured at 77 K with a Micromeritics Tristar-3000 analyzer. Each sample was degassed for 1 h at 90°C and another 3 h at 300°C under N₂ atmosphere before the measurement. The specific surface area was calculated using standard BET method at a relative pressure (P/P₀) range of 0.05–0.35 and the V-t plot method was utilized to calculate the pore volume.

The morphology of the catalysts was observed by the field emission scanning electron microscope (FESEM, Nanosem 430). X-ray photoelectron spectroscopy (XPS) analysis was conducted with a PHI-1600 instrument using Mg K α radiation (1253.6 eV) as X-ray source. TEM observations were carried out using a Tecnai G² F-20 transmission electron microscope with a field-emission gun operating at 200 kV.

Results and discussion

The influence of ion exchange level on NH₃-SCR activity

The catalytic activity of Ce_x-Fe_y/Cu-SSZ-13 (x=0~0.15, y=0.017) were studied from 150□ to 550□ under 150000 h⁻¹. Fig. 1(a) shows NO conversion vs temperature. The NO conversion over Ce_x-Fe_y/Cu-SSZ-13 (x=0.006~0.15, y=0.017) increased rapidly below 200 □ and reached above 90% in the temperature range of 200 □ to 500 □. Especially within the temperature range of 150 to 225□, NO conversion increased significantly with x increasing from 0 to 0.017. For example, the

NO conversion over $\text{Ce}_0\text{-Fe}_{0.017}/\text{Cu-SSZ-13}$ and $\text{Ce}_{0.017}\text{-Fe}_{0.017}/\text{Cu-SSZ-13}$ at 175°C are 76.8% and 86.2%, respectively. However, there was only a little increase of NO conversion with x increasing from 0 to 0.017 within the temperature range of 250 to 550°C . In addition, NO conversion decreased with x increasing from 0.017 to 0.15 between 150°C and 550°C due to the blocking of the “channel” of zeolites¹². Clearly, $\text{Ce}_{0.017}\text{-Fe}_{0.017}/\text{Cu-SSZ-13}$ showed the best catalytic activity in a wider operation temperature window from 150 to 550°C . As presented in Fig. 1(b), there was almost no NO_2 in the outlet gases and the concentration of N_2O was less than 6 ppm. Obviously, the concentration of N_2O reached the maximum value at 250°C , which was correspond to the lowest N_2 selectivity. Fig. 1(b) also showed that N_2 selectivity over $\text{Ce}_{0.017}\text{-Fe}_{0.017}/\text{Cu-SSZ-13}$ catalyst was above 98% in the temperature between 150°C and 550°C , which made Ce-Fe /Cu-SSZ-13 catalyst as a promising candidate for NH_3 -SCR technology.

Effects of GHSV on NH_3 -SCR Activity

The NH_3 -SCR catalyst in diesel vehicles usually undergoes different GHSV in the practical application. Fig. 2 showed NO conversion over $\text{Ce}_{0.017}\text{-Fe}_{0.017}/\text{Cu-SSZ-13}$ under different GHSV. It was clear that with the increase of GHSV from $60\,000\text{ h}^{-1}$ to $300\,000\text{ h}^{-1}$, NO conversion decreased significantly at low temperature below 200°C , yet there was only a little effect on the higher temperature ($225\text{-}350^\circ\text{C}$) SCR activity. Especially within the temperature range of 400°C to 550°C , there almost no effect on NO conversion. Remarkably, the catalyst showed high NO conversion exceeding 90% during the temperature range of 225 to 500°C under a rather high GHSV of $300\,000\text{ h}^{-1}$, indicating that this catalyst is effectively resistant against high space velocity.

The effect of O_2 concentration on the SCR activity

The influence of O_2 concentration on NO conversion over $\text{Ce}_{0.017}\text{-Fe}_{0.017}/\text{Cu-SSZ-13}$ catalyst

was investigated at 300 °C under 150 000 h⁻¹ and the result was exhibited in Fig. 3. The NO conversion increased from 75.6% to 99.4% with the concentration of O₂ increasing from 0 to 3 vol%. The increased catalytic activity might be related to the role that O₂ played in the reaction. Two possible explanations may be that the main role of O₂ is H-abstraction from adsorbed NH₃, resulting in NH₂ species, and secondly, O₂ can be needed to react with NO to form an active intermediate species¹⁶⁻¹⁸. However, as the concentration of O₂ continued to increase, NO conversion remained unchanged indicating that O₂ is saturated.

The Influences of SO₂, CO₂ and H₂O on NH₃-SCR activity

Fig. 4(a) shows the effects of H₂O and SO₂ on the catalytic activity of Ce_{0.017}-Fe_{0.017}/Cu-SSZ-13 catalyst at 300 °C under 150000 h⁻¹. When 5 vol% H₂O was added, the activity of the catalyst remained at the previous high level at 300 °C. This suggested that the catalyst was highly water-resistant under these SCR conditions. When 100 ppm SO₂ was added into the feed gases, there was a slight decrease of the NO conversion. The decrease was attributed to the competitive adsorption between SO₂ and NO¹⁹, so the conversion was restored to its original level after removing SO₂. However, when 100 ppm SO₂ and 5 % H₂O were injected into the reaction system simultaneously, NO conversion decreased considerably compared with only 100 ppm SO₂ or 5 vol% H₂O, which might be related to the formation of sulfates that could poison the active sites or block the zeolite pores and the competitive adsorption between SO₂ and NO on the active sites²⁰. The effects of H₂O and CO₂ on the catalytic activity of Ce_{0.017}-Fe_{0.017}/Cu-SSZ-13 catalyst were illustrated in Fig. 4(b). It was clear that pure CO₂ and the co-presence of CO₂ and H₂O in feed gases almost had no effect on NO conversion.

Fig. 5 shows the effect of Ce doping on SO₂ resistance. It is clear that Ce-doped catalyst

(Ce_{0.017}-Fe_{0.017}/Cu-SSZ-13) showed a remarkable enhancement in sulfur-water tolerance compared with Ce₀-Fe_{0.017}/Cu-SSZ-13. The improvement of sulfur tolerance might be attributed to that the doping of Ce could efficiently retard the formation of surface sulfation species²¹.

Fig. 6 shows the effect of temperature on SO₂ resistance of Ce_{0.017}-Fe_{0.017}/Cu-SSZ-13. A continuous decline in NO conversion from 99.4% to 66.6% occurred after 100 ppm SO₂ and 5 vol% H₂O were added for 12 h at 300 °C. When the temperature was maintained at 350 °C, NO conversion decreased from 95% to 86.8% after 100 ppm SO₂ and 5 vol% H₂O were added for 1 h, then the NO conversion became stable for another 11 h. The deactivation role of SO₂ over the catalyst might be related to the formation of ammonium sulfate. (NH₄)₂SO₄ decomposition involves the initial decomposition to NH₃ and NH₄HSO₄ at around 300 °C and the subsequent decomposition of surface NH₄HSO₄ species to NH₃ and SO₂ at 350 °C.^{20,22} After removal of SO₂ and H₂O, NO conversion restored to some extent at both 300 °C and 350 °C. Obviously, there was almost no effect of SO₂ and H₂O on the NO conversion when the temperature is higher than 400 °C. The results above suggested that the impact of SO₂ on NO conversion could be eliminated by increasing temperature.

The results of TEM

Fig. 7 shows the TEM micrographs of Ce_{0.006}-Fe_{0.017}/Cu-SSZ-13, Ce_{0.017}-Fe_{0.017}/Cu-SSZ-13 and Ce_{0.15}-Fe_{0.017}/Cu-SSZ-13. The small dark spots were attributed to oxide metal nanoparticles (CeO₂, α-Fe₂O₃ and CuO) and the faint background represented the SSZ-13 support. It could be clearly seen that, oxide metal nanoparticles were well dispersed on the surface of the catalysts.

XRD patterns results

The XRD patterns of Ce_x-Fe_y/Cu-SSZ-13 catalysts and JCPDS reference of SSZ-13 were shown in Fig. 8. All catalysts exhibited the characteristic peaks corresponding to SSZ-13 zeolite

structure ($2\theta = 9.5^\circ, 14.0^\circ, 16.1^\circ, 17.8^\circ, 20.7^\circ, 25.0^\circ, 26.1^\circ$ and 30.9°) with a perfect degree of crystallization, indicating that the original zeolite structure remained intact. The diffraction peaks of CeO_2 , $\alpha\text{-Fe}_2\text{O}_3$ and CuO were not observed among all catalysts, indicating that the copper, iron and cerium species as oxide metal nanoparticles were well dispersed on the surface of SSZ-13 support, which was confirmed by the results of TEM images.

The results of BET

Fig. 9 showed the results of N_2 adsorption-desorption isotherms and pore-size distribution of $\text{Ce}_x\text{-Fe}_y/\text{Cu-SSZ-13}$ catalysts. According to the IUPAC classification, all adsorption-desorption isotherm curves of the samples in Fig. 9(a) can be considered as a combination of type I and type IV, indicating the presence of microporous and slit shaped pores. Fig. 9(b) showed that $\text{Ce}_0\text{-Fe}_{0.017}/\text{Cu-SSZ-13}$, $\text{Ce}_{0.006}\text{-Fe}_{0.017}/\text{Cu-SSZ-13}$, $\text{Ce}_{0.017}\text{-Fe}_{0.017}/\text{Cu-SSZ-13}$ and $\text{Ce}_{0.15}\text{-Fe}_{0.017}/\text{Cu-SSZ-13}$ catalysts had only a narrow visible peak at around 3.94nm, 3.99nm, 3.92nm, and 4.38nm respectively, indicating that excessive loading of Ce resulted in larger pore size. The pore structure parameters of all samples were listed in Table1. It is clear that the surface area and pore volume of $\text{Ce}_x\text{-Fe}_y/\text{Cu-SSZ-13}$ catalysts decreased with the increasing of cerium content indicating that excessive Ce loading results in agglomeration that blocked the “channel” of catalysts. Remarkably, $\text{Ce}_{0.006}\text{-Fe}_{0.017}/\text{Cu-SSZ-13}$ and $\text{Ce}_{0.017}\text{-Fe}_{0.017}/\text{Cu-SSZ-13}$ catalysts with larger surface area and smaller pore size exhibited higher catalytic activity compared with $\text{Ce}_{0.15}\text{-Fe}_{0.017}/\text{Cu-SSZ-13}$ catalyst combined with Fig. 1 and Table 1. The results were in accordance with the previous report that larger specific surface areas and smaller pore size were in favor of catalytic reaction²³.

The results of SEM

The SEM micrographs of $\text{Ce}_{0.017}\text{-Fe}_{0.017}/\text{Cu-SSZ-13}$ are shown in Fig. 10. It is clear that the sample was made of hexagonal crystal. The average particle size of the catalyst is about $2.5\mu\text{m}$. In addition, It can be seen from the image that the catalyst shows perfect degree of crystallization which is in accordance with the results of XRD.

The metal dispersion

The metal dispersion of $\text{Ce}_{0.017}\text{-Fe}_{0.017}/\text{Cu-SSZ-13}$ determined by XPS and ICP was shown in Table 2. It is clear that Fe and Ce species are mostly dispersed on the surface of the catalyst $\text{Ce}_{0.017}\text{-Fe}_{0.017}/\text{Cu-SSZ-13}$ through post-synthesis cation exchanges. The good metal dispersion was favorable to the synergetic effects.

Conclusions

A series of CHA-type trimetallic composite zeolites of $\text{Ce}_x\text{-Fe}_y/\text{Cu-SSZ-13}$ catalysts were prepared by the one-pot synthesized Cu-SSZ-13 and subsequent ion-exchange with Fe^{3+} and Ce^{3+} . The results of XRD revealed that the zeolite structure remained intact after both Fe and Ce incorporation into Cu-SSZ-13. The SEM micrographs showed that the sample was made of hexagonal crystal. $\text{Ce}_{0.017}\text{-Fe}_{0.017}/\text{Cu-SSZ-13}$ have a large BET specific surface area ($503\text{ m}^2/\text{g}$) and a narrow pore size distribution (3.92 nm). Excessive Ce loading would result in agglomeration that blocked the “channel” of catalysts. Larger specific surface areas and smaller pore size were in favor of catalytic reaction, which can be concluded combined catalytic performance tests with the results of BET. Among the prepared $\text{Ce}_x\text{-Fe}_y/\text{Cu-SSZ-13}$ catalysts, $\text{Ce}_{0.017}\text{-Fe}_{0.017}/\text{Cu-SSZ-13}$ catalyst showed the best catalytic performance. The good metal dispersion of $\text{Ce}_{0.017}\text{-Fe}_{0.017}/\text{Cu-SSZ-13}$ was favorable to the synergetic effects. It presented super $\text{NH}_3\text{-SCR}$ activity, excellent N_2 selectivity in a relatively wide temperature range, strong resistance to high space velocity as well as good tolerance

to CO₂ and H₂O. In addition, Ce_{0.017}-Fe_{0.017}/Cu-SSZ-13 (Ce-doped catalyst) showed a remarkable enhancement in sulfur-water tolerance compared with Ce₀-Fe_{0.017}/Cu-SSZ-13. The impact of SO₂ on NO conversion could be eliminated by increasing temperature. Further studies on the mechanism of the reaction are in progress.

References

1. P. Granger and V. I. Parvulescu, *Chem. Rev.*, 2011, 111, 3155-3207.
2. U. Deka, I. Lezcano-Gonzalez, S. J. Warrender, A. L. Picone, P. A. Wright, B. M. Weckhuysen and A. M. Beale, *Microporous Mesoporous Mater.*, 2013, 166, 144-152.
3. X. F. Yang, Z. L. Wu, M. Moses-Debusk, D. R. Mullins, S. M. Mahurin, R. A. Geiger, M. Kidder and C. K. Narula, *J. Phys. Chem. C*, 2012, 116, 23322-23331.
4. J. H. Kwak, R. G. Tonkyn, D. H. Kim, J. Szanyi and C. H. F. Peden, *J. Catal.*, 2010, 275, 187-190.
5. S. J. Schmiege, S. H. Oh, C. H. Kim, D. B. Brown, J. H. Lee, C. H. F. Peden and D. H. Kim, *Catal. Today*, 2012, 184, 252-261.
6. *US Pat.*, 4 544 538, 1985.
7. S. I. Zones, *J. Chem. Soc., Faraday Trans.*, 1991, 87, 3709-3716.
8. N. Martín, M. Moliner and A. Corma, *Chem. Commun.*, 2015, 51, 9965-9968.
9. B. H. Chen, R. N. Xu, R. D. Zhang and N. Liu, *Environ. Sci. Technol.*, 2014, 48, 13909-13916.
10. L. M. Ren, L. F. Zhu, C. G. Yang, Y. M. Chen, Q. Sun, H. Y. Zhang, C. J. Li, F. Nawaz, X. J. Meng and F. S. Xiao, *Chem. Commun.*, 2011, 47, 9789-9791.
11. L. J. Xie, F. D. Liu, L. M. Ren, X. Y. Shi, F. S. Xiao and H. He, *Environ. Sci. Technol.*, 2014, 48, 566-572.

12. R. R. Zhang, Y. H. Li and T. L. Zhen, *RSC Adv.*, 2014, 4, 52130-52139.
13. X. Gao, Y. Jiang, Y. C. Fu, Y. Zhong, Z. Y. Luo and K. Cen, *Catal. Commun.*, 2010, 11, 465-469.
14. E. Ito, Y. J. Mergler, B. E. Nieuwenhuys, H. V. Bekkum and C. M. V. D. Bleek, *Microporous Mater.*, 1995, 4, 455-465.
15. T. T. Gu, Y. Liu, X. L. Weng, H. Q. Wang and Z. B. Wu, *Catal. Commun.*, 2010, 12, 310-313.
16. K. S. Kijlstra, D. S. Brands, H. I. Smit, E. K. Poels and A. Bliet, *J. Catal.*, 1997, 171, 219-230.
17. K. S. Kijlstra, D. S. Brands, E. K. Poels and A. Bliet, *J. Catal.*, 1997, 171, 208-218.
18. H. Sjövall, L. Olsson, E. Fridell and R. J. Blint, *Appl. Catal., B*, 2006, 64, 180-188.
19. Y. T. Li and Q. Zhong, *J. Hazard. Mater.*, 2009, 172, 635-640.
20. L. Zhang, D. Wang, Y. Liu, K. Kamasamudram, J. H. Li and W. Epling, *Appl. Catal., B*, 2014, 156, 371-377.
21. R. B. Jin, Y. Liu, Y. Wang, W. L. Cen, Z. B. Wu, H. Q. Wang and X. L. Weng, *Appl. Catal., B*, 2014, 148, 582-588.
22. I. S. Nam, J. W. Eldridge and J. R. Kittrell, *Ind. Eng. Chem. Prod. Res. Dev.*, 1986, 25, 192-197.
23. J. H. Park, H. J. Park, J. H. Baik, I. S. Nam, C. H. Shin, J. H. Lee, B. K. Cho and S. H. Oh, *J. Catal.*, 2006, 240, 47-57.

Figure captions

Fig.1 NO conversion over $Ce_x-Fe_y/Cu-SSZ-13$ catalysts under GHSV of 150000 h^{-1} (a), N_2 selectivity of $Ce_{0.017}-Fe_{0.017}/Cu-SSZ-13$ catalyst (b).

Fig.2 NH_3 -SCR activity over $Ce_{0.017}-Fe_{0.017}/Cu-SSZ-13$ under different GHSV

Fig. 3 NH_3 -SCR activity over $Ce_{0.017}-Fe_{0.017}/Cu-SSZ-13$ catalyst at $300\text{ }^\circ\text{C}$ under GHSV of $150\ 000\text{ h}^{-1}$ at different O_2 concentration

Fig. 4 NO conversion over $Ce_{0.017}-Fe_{0.017}/Cu-SSZ-13$ catalyst at $300\text{ }^\circ\text{C}$ under GHSV of $150\ 000\text{ h}^{-1}$ in the co-presence of $H_2O + SO_2$ (a); $H_2O + CO_2$ (b).

Fig.5 NO conversion over $Ce_0-Fe_{0.017}/Cu-SSZ-13$ and $Ce_{0.017}-Fe_{0.017}/Cu-SSZ-13$ at $300\text{ }^\circ\text{C}$ under GHSV of $150\ 000\text{ h}^{-1}$ in the co-presence of $H_2O + SO_2$

Fig.6 NO conversion over $Ce_{0.017}-Fe_{0.017}/Cu-SSZ-13$ at different temperature under GHSV of $150\ 000\text{ h}^{-1}$ in the co-presence of $H_2O + SO_2$

Fig.7 TEM images of $Ce_{0.006}-Fe_{0.017}/Cu-SSZ-13$ (a), $Ce_{0.017}-Fe_{0.017}/Cu-SSZ-13$ (b) and $Ce_{0.15}-Fe_{0.017}/Cu-SSZ-13$ (c)

Fig.8 XRD patterns of $Ce_x-Fe_y/Cu-SSZ-13$ catalysts and JCPDS reference of SSZ-13 zeolite

Fig. 9 N_2 adsorption-desorption isotherms (a) and pore-size distribution curves (b) of $Ce_x-Fe_y/Cu-SSZ-13$ catalysts

Fig. 10 SEM images of $Ce_{0.017}-Fe_{0.017}/Cu-SSZ-13$

Table 1 The physicochemical properties of $Ce_x-Fe_y/Cu-SSZ-13$ catalysts

Table 2 Metal dispersion (%) of $Ce_{0.017}-Fe_{0.017}/Cu-SSZ-13$

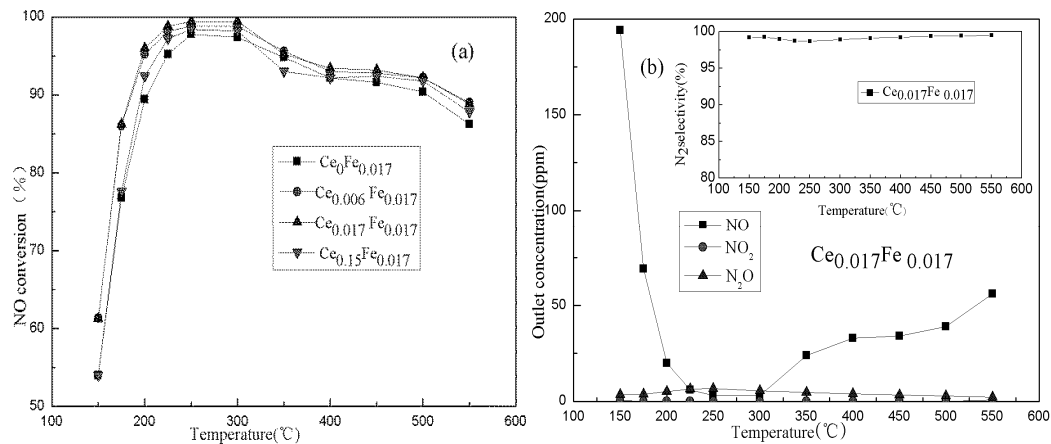


Fig.1 NO conversion over $Ce_x-Fe_y/Cu-SSZ-13$ catalysts under GHSV of $150000\ h^{-1}$ (a), N_2 selectivity of $Ce_{0.017}-Fe_{0.017}/Cu-SSZ-13$ catalyst (b).

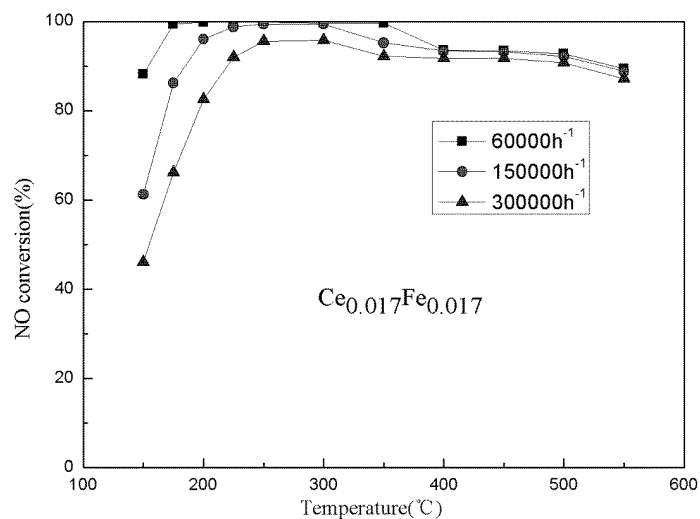


Fig.2 NH_3 -SCR activity over $Ce_{0.017}-Fe_{0.017}/Cu-SSZ-13$ under different GHSV

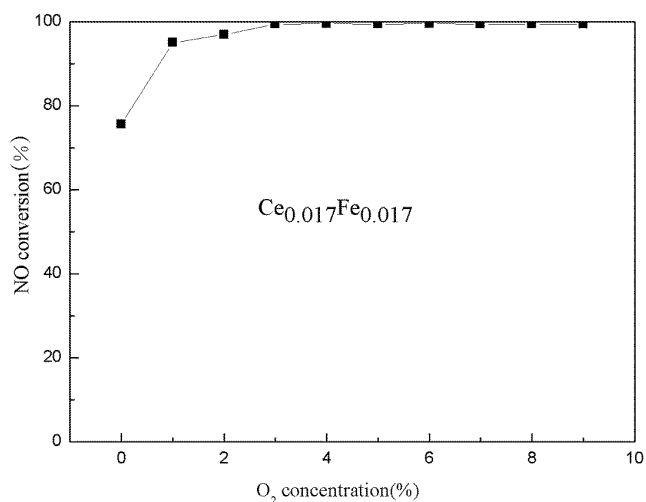


Fig. 3 NH₃-SCR activity over Ce_{0.017}-Fe_{0.017} /Cu-SSZ-13 catalyst at 300 °C under GHSV of 150 000 h⁻¹ at different O₂ concentration

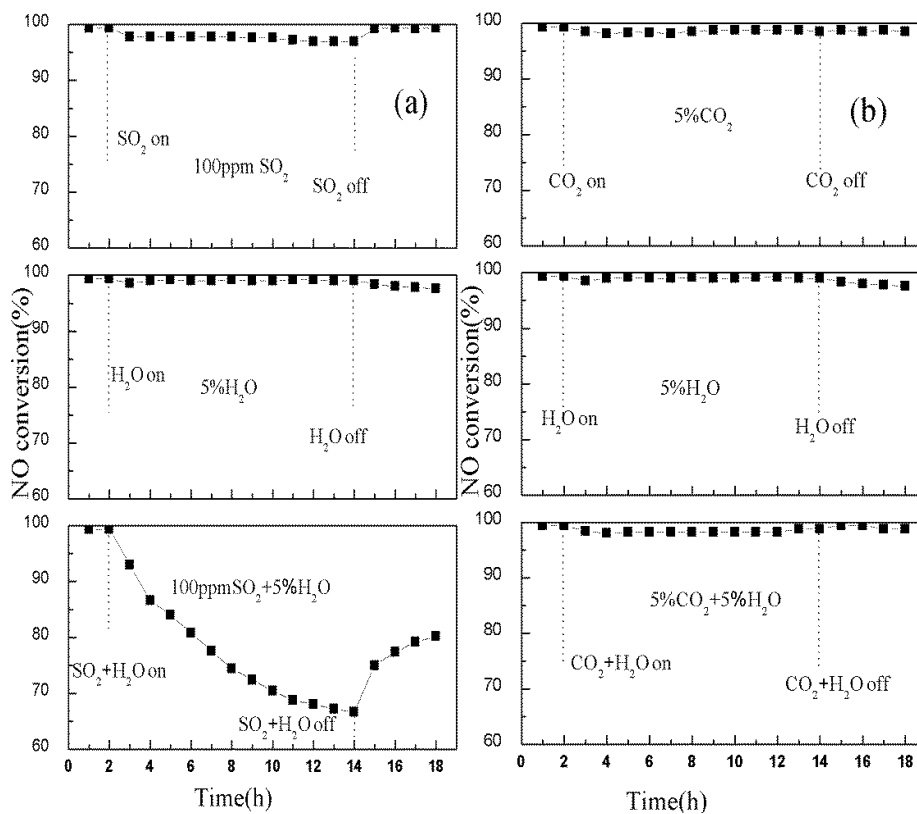


Fig. 4 NO conversion over Ce_{0.017}-Fe_{0.017} /Cu-SSZ-13 catalyst at 300 °C under GHSV of 150 000 h⁻¹ in the co-presence of H₂O + SO₂ (a); H₂O + CO₂ (b).

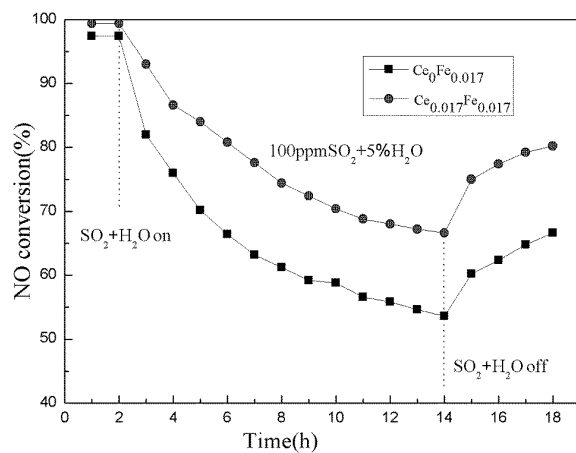


Fig.5 NO conversion over $Ce_0-Fe_{0.017}/Cu-SSZ-13$ and $Ce_{0.017}-Fe_{0.017}/Cu-SSZ-13$ at 300 °C under GHSV of $150\,000\ h^{-1}$ in the co-presence of $H_2O + SO_2$

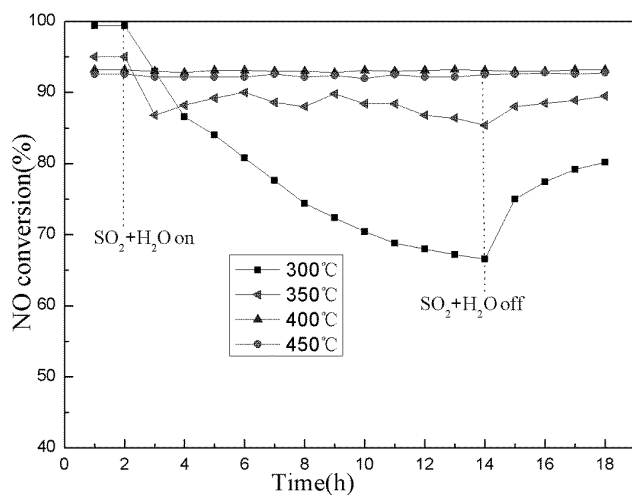


Fig.6 NO conversion over $Ce_{0.017}-Fe_{0.017}/Cu-SSZ-13$ at different temperature under GHSV of $150\,000\ h^{-1}$ in the co-presence of $H_2O + SO_2$

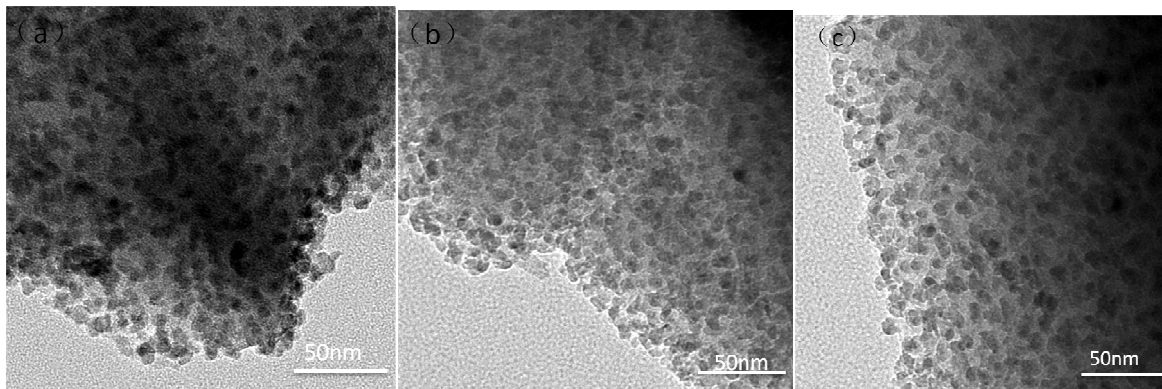


Fig. 7 TEM images of $\text{Ce}_{0.006}\text{-Fe}_{0.017}/\text{Cu-SSZ-13}$ (a), $\text{Ce}_{0.017}\text{-Fe}_{0.017}/\text{Cu-SSZ-13}$ (b) and $\text{Ce}_{0.15}\text{-Fe}_{0.017}/\text{Cu-SSZ-13}$ (c)

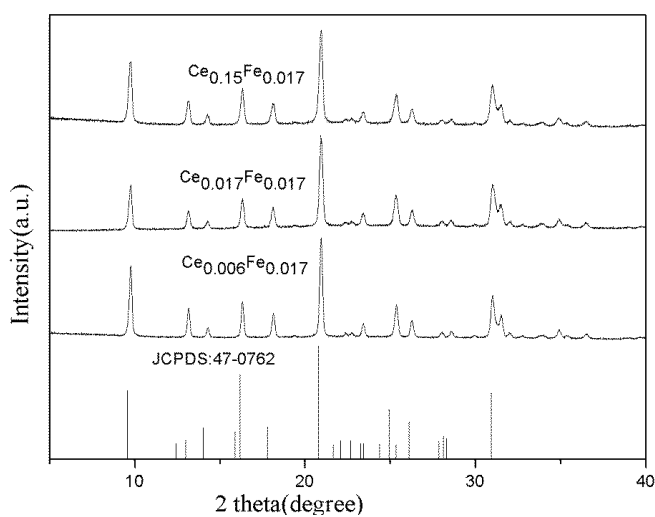


Fig.8 XRD patterns of $\text{Ce}_x\text{-Fe}_y/\text{Cu-SSZ-13}$ catalysts and JCPDS reference of SSZ-13 zeolite

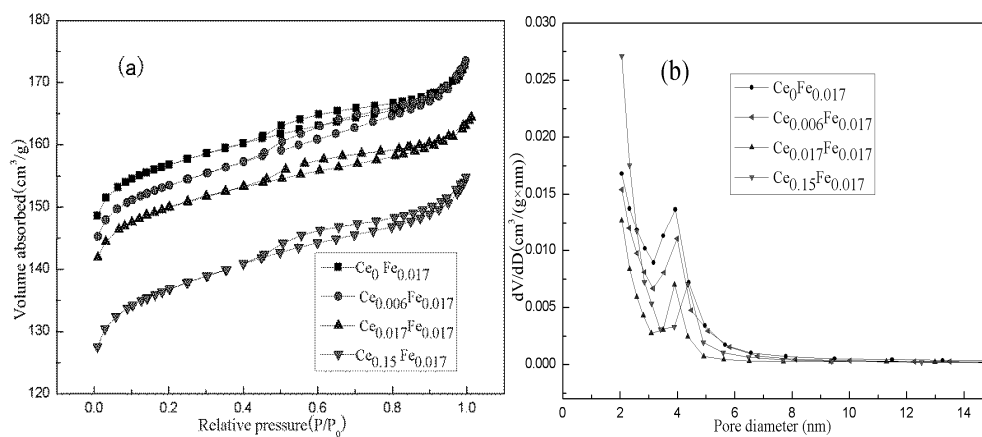


Fig. 9 N_2 adsorption-desorption isotherms (a) and pore-size distribution curves (b) of $\text{Ce}_x\text{-Fe}_y/\text{Cu-SSZ-13}$ catalysts

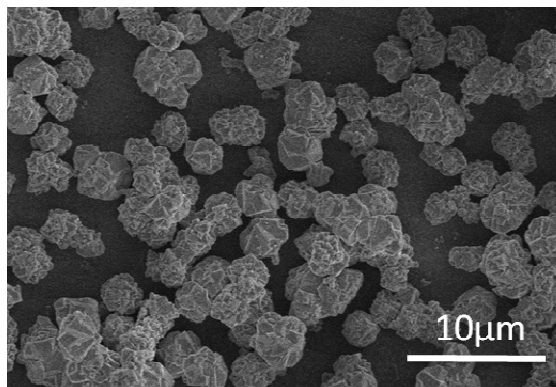


Fig. 10 SEM images of $\text{Ce}_{0.017}\text{-Fe}_{0.017}/\text{Cu-SSZ-13}$

Table 1 The physicochemical properties of $\text{Ce}_x\text{-Fe}_y/\text{Cu-SSZ-13}$ catalysts

Sample	S_{BET} (m^2/g) ^a	Pore volume (cm^3/g) ^b	Average pore diameter (nm) ^c	Concentration(wt%) ^d		
				Ce	Fe	Cu
$\text{Ce}_0\text{-Fe}_{0.017}/\text{Cu-SSZ-13}$	522	0.220	3.90	–	3.44	1.27
$\text{Ce}_{0.006}\text{-Fe}_{0.017}/\text{Cu-SSZ-13}$	511	0.214	3.97	0.67	3.10	1.11
$\text{Ce}_{0.017}\text{-Fe}_{0.017}/\text{Cu-SSZ-13}$	503	0.194	3.91	0.82	3.48	1.14
$\text{Ce}_{0.15}\text{-Fe}_{0.017}/\text{Cu-SSZ-13}$	458	0.186	4.31	0.87	3.28	1.10

a Calculated by BET method.

b Calculated by t-plot method.

c Calculated using the BJH method with desorption branch.

d Characterized by ICP-OES.

Table 2 Metal dispersion (%) of $\text{Ce}_{0.017}\text{-Fe}_{0.017}/\text{Cu-SSZ-13}$

Sample	metal dispersion (%) ^a		
	Ce	Fe	Cu
$\text{Ce}_{0.017}\text{-Fe}_{0.017}/\text{Cu-SSZ-13}$	84.76	100	25.09

a metal dispersion(%)=the number of metal atoms on the surface/ total number of metal atoms in the bulk